Sensitivity of the CFD Mesh for a Single Rising Bubble in a Hallimond Tube

Ashraf Azmi[1,a], Periyasamy Balasubramanian[1,b], Bawadi Abdullah[1,c], Ehsan Zhalehrajabi[1,d]

[1]Chemical Engineering Department, Universiti Teknologi PETRONAS, Bandar Seri Iskandar, 31750 Tronoh, Perak Darul Ridzuan, Malaysia.

[a]ashrafazmi88@gmail.com,[b]periyasamy.b@petronas.com.my, [c]bawadi_abdullah@petronas.com.my, [d]ehsan_g01985@utp.edu.my

Keywords: Rising bubble; Flotation; Hallimond tube; CFD

Abstract. This paper presents how a single rising bubble experiment in the Hallimond Tube (HT) can be predicted using a computational fluid dynamics model (CFD). The study is emphasized on the effect of CFD Mesh to the pressure coefficient and axial velocity around the bubble. A rigid sphere with the radius of 0.00575 m using flow velocity of 0.0067 m/s was considered in this study. Experimental and simulated data obtained by other researchers in the similar study were used to validate the simulation results from the computational fluid dynamics model.

Introduction

Rising bubble phenomena is related to flotation, which is widely used by mineral and chemical engineers for the separation and concentration of aqueous suspensions or solutions of a variety of minerals, precipitates, inorganic waste constituents, and even microorganisms and proteins [1, 2]. It is now well established that the recovery of particles by flotation is most successful in 10-200 μm size range [3, 4]. In these range particles are susceptible to dynamic effect around a rising bubble [5], therefore, dynamics study around a bubble is essential for an accurate prediction of bubble-particle collision efficiency.

The actual flotation of mineral particles depends on a large number of interacting variables [6]. Therefore, understanding the characteristics of a rising bubble in water is very important in a flotation process. A laboratory scale flotation device is required in which chemical and mechanical variables can be closely controlled. One of such device used for this purpose is Hallimond Tube (HT) as shown in Figure 1. HT is a fairly well accepted method for testing of flotability in which the bubble rising toward the surface of the water.

Since bigger bubbles experience shape deformation [7] and zigzag motion [8], and this will cause more complications to the study. Therefore, a small rigid sphere is considered in the present work to circumvent this problem. The computational fluid dynamics (CFD) model is designed solely based on the HT characterization (see Figure 2). Earlier, CFD model was used to study the plume of bubble, however the dynamics around a single bubble and effect of aspect ratio (AR) are not available in the literature.

Therefore, a CFD model is developed to study the hydrodynamic of a rising bubble in HT. Furthermore, CFD model was implemented using Star-CCM+ V6.04[®] to determine the dynamics around a single bubble and to investigate effect of mesh to the single rising bubble inside HT.
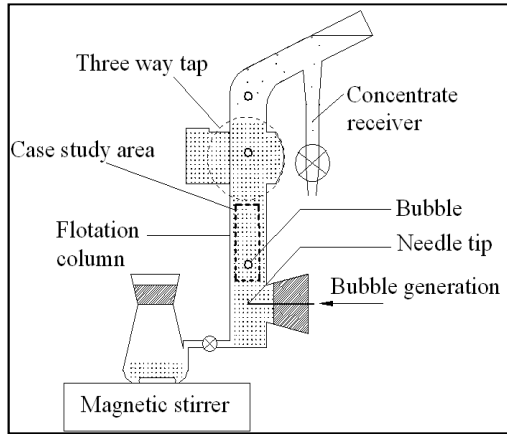
Fig. 1. Schematic diagram of the Hallimond Tube.
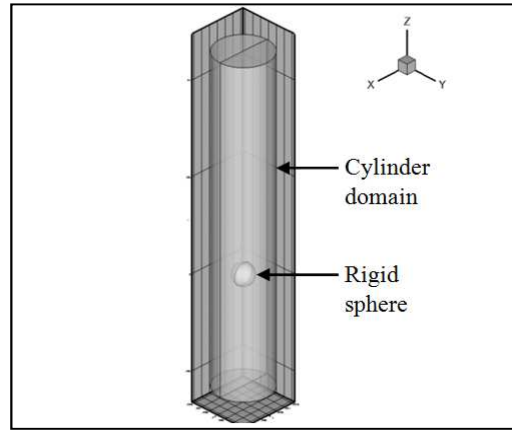
Fig. 2. Schematic diagram of the CFD domain.

Model descriptions and test cases

On a single rising bubble in HT study, primary flow was solved. In order to get Reynold's number (Re=100), bubble rising velocity was set as 0.0067 m/s. Since, in this simulation, a static spherical solid was used instead of rising bubble, therefore, velocity of 0.0067 m/s was used as water flow velocity in order to match the phenomena of bubble rising in Hallimond Tube. Location of spherical solid was kept fixed at (0,0,0).

Table 1. Descbubble. However, ation Test.

Meshing, M Cell size (m)	Test 1 (M1)	TCFD mesh	Test 3 (M3)
Maximum	0.0030 m	0.0030 m	0.0030 m
Minimum	0.0009 m	0.00075 m	0.0006 m

Mesh parameters for validation and descriptions of test cases are listed in Table 1. Mesh refinement around the spherical solid was achieved with volumetric control size adjustment. Figure 3 show the schematic diagram of the M1, M2 and M3 mesh.
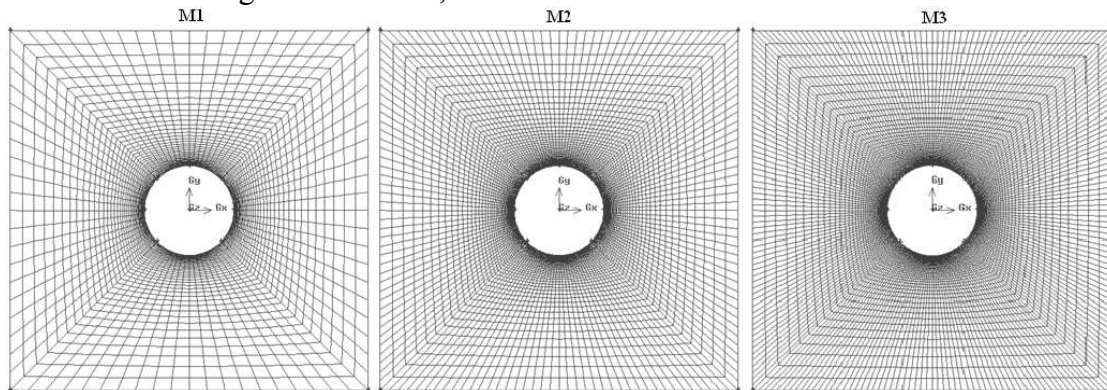
Fig. 3. 2-D view of meshing around spherical solid

For the model equation, the steady-state Navier-Stokes continuous equation (Eq. 1) and momentum equation (Eq. 2-4) for primary flow in cylindrical coordinates are described below. The steady-state Navier-Stokes continuous equation in three-dimensional is given by eq. 1

$$\frac{\partial \rho}{\partial t} + \frac{1}{r}\frac{\partial}{\partial r}(\rho r v_r) + \frac{1}{r}\frac{\partial}{\partial \theta}(\rho v_\theta) + \frac{\partial}{\partial z}(\rho v_z) = 0 \tag{1}$$

where, ρ is fluid density, r is cylinder radius, v_r, v_θ, and v_z are fluid velocity in r-direction, θ-direction, and z-direction. The steady-state Navier-Stokes momentum balance equation in the r-direction is given by eq. 2

$$\rho\left(\frac{\partial v_r}{\partial t}+v_r\frac{\partial v_r}{\partial r}+\frac{v_\theta}{r}\frac{\partial v_r}{\partial \theta}+v_z\frac{\partial v_r}{\partial z}-\frac{v_\theta^2}{r}\right)=-\frac{\partial p}{\partial r}+\mu\left[\frac{\partial}{\partial r}\left(\frac{1}{r}\frac{\partial}{\partial r}(rv_r)\right)+\frac{1}{r^2}\frac{\partial^2 v_r}{\partial \theta^2}+\frac{\partial^2 v_r}{\partial z^2}-\frac{2}{r^2}\frac{\partial v_\theta}{\partial \theta}\right]+\rho g_r \quad (2)$$

where, μ is fluid kinematic viscosity, g is gravitational acceleration. The steady-state Navier-Stokes momentum balance equation in the θ-direction is given by eq. 3

$$\rho\left(\frac{\partial v_\theta}{\partial t}+v_r\frac{\partial v_\theta}{\partial r}+\frac{v_\theta}{r}\frac{\partial v_\theta}{\partial \theta}+v_z\frac{\partial v_\theta}{\partial z}+\frac{v_r v_\theta}{r}\right)=-\frac{1}{r}\frac{\partial p}{\partial \theta}+\mu\left[\frac{\partial}{\partial r}\left(\frac{1}{r}\frac{\partial}{\partial r}(rv_\theta)\right)+\frac{1}{r^2}\frac{\partial^2 v_\theta}{\partial \theta^2}+\frac{\partial^2 v_\theta}{\partial z^2}+\frac{2}{r^2}\frac{\partial v_r}{\partial \theta}\right]+\rho g_\theta \quad (3)$$

The state Navier-Stokes momentum balance equation in the z-direction is given by eq. 4

$$\rho\left(\frac{\partial v_z}{\partial t}+v_r\frac{\partial v_z}{\partial r}+\frac{v_\theta}{r}\frac{\partial v_z}{\partial \theta}+v_z\frac{\partial v_z}{\partial z}\right)=-\frac{\partial p}{\partial z}+\mu\left[\frac{1}{r}\frac{\partial}{\partial r}\left(r\frac{\partial v_z}{\partial r}\right)+\frac{1}{r^2}\frac{\partial^2 v_z}{\partial \theta^2}+\frac{\partial^2 v_z}{\partial z^2}\right]+\rho g_z \quad (4)$$

All the above-mentioned model equations were solved using Star CCM.

Results and Discussion

Figure 4 show pressure coefficient, C_p around a bubble versus the angular position of the bubble surface. The surface angle θ, considered for this study is between 0° to 180°. Experimental data [8] and simulation data [9] is used for mesh validation. This part of the research is carried out to improve confidence in the CFD prediction on the bubble surface.

Assuming the solution is in the laminar flow regime and at steady state, three refined mesh sizes around the surface of the spherical solid are used as a part of grid independent test. Grid-independent test is a crucial process in determining the accuracy of the solution. Grid independent solution is obtained for all the meshes.

From the simulation test result shown in Figure 4, little difference is shown from M1, M2 and M3 plot. However, a significant difference is observed for M3 plot. At the vicinity of 116.6°, C_p for M3 starts to decrease gradually until the end point. Highest C_p difference is observed at angular position of 128.7°. Taken M2 as the reference mesh, the percentage of difference between M3 and M2 at this point is 28.9%. It is evident that effect of mesh is significant to the value of C_p.
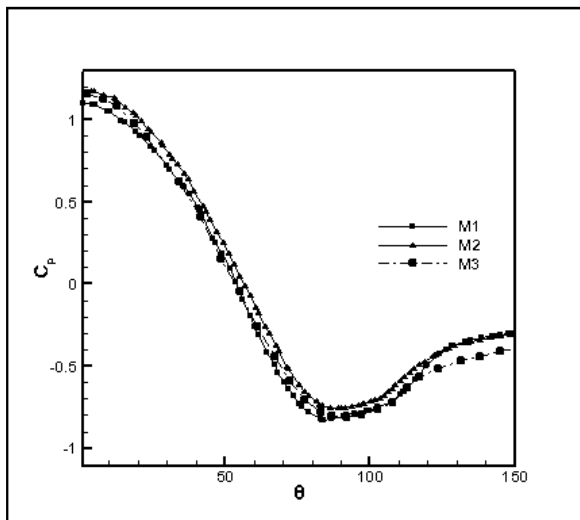
Fig. 4. Pressure coefficient comparison for flow around a spherical solid with different meshes.
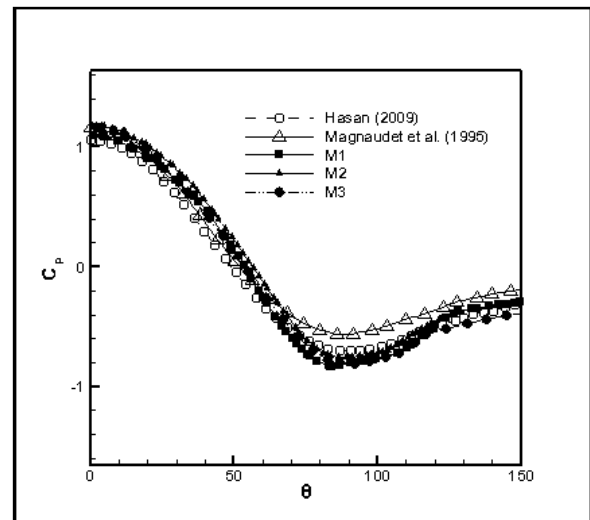
Fig. 5. Validation with experimental [10] and computational [9] data.

In this study, M3 is having the finest mesh, however, it shows the highest C_p diversion from experimental results [8] as shown in Figure 5. From preliminary observation, suppose, a finer mesh should give closer agreement between simulated and experimental results, but in this case study, it is known that using finer mesh causing instability in a solution convergence thus affected the value of the pressure coefficients at the specific iteration no.

The results for case validation from Test 1, Test 2, and Test 3 are compared and shown in Figure 5. Here, it is observed that M2 mesh shows best fit with the experiment data [8] and simulation data predicted by [9]. From this result, it is assumed that cell size (minimum) of 0.00075 m M2 provides more accurate solution as compared to the other cell size (minimum).

Conclusions

For the effect of mesh on the fluid characterization around the bubble, 210 divisions around the spherical solid periphery were required to attain grid independent solution. Only cell size of M2 and M3 managed to provide more than 200 divisions. Using a finer mesh offered closer agreement between simulated and experimental results. However, in this study, it is found that using finer mesh (M3) causing instability in a solution.

Acknowledgement

Reference

[1] Y. Liang, N. Hilal, Interaction forces between colloidal particles in liquid: Theory and experiment, Advances in Colloid and Interface Science 134 (2007) 151–166.

[2] T. Miettinen, J. Ralston, The limits of fine particle flotation, Minerals Engineering 23 (2010) 420–437.

[3] Z. Dai, D. Fornasiero, J. Ralston, Particle–bubble collision models — a review, Advances in Colloid and Interface Science 85 (2000) 231-256.

[4] S. Yang, R. Pelton, A. Raegen, M. Montgomery, K. Dalnoki-Veress, Nanoparticle Flotation Collectors: Mechanisms Behind a New Technology, Langmuir 27 (2011) 10438–10446.

[5] R.H. Yoon, The role of hydrodynamic and surface forces in bubble–particle interaction, Int. J. Miner. Process. 58 (2000) 129-143.

[6] D.I. Verrelli, P.T.L. Koh, Particle–bubble interaction and attachment in flotation, Chemical Engineering Science 66 (2011) 5910-5921.

[7] G. Bozzano, and M. Dente, Shape and terminal velocity of single bubble motion: A novel approach, Computers & Chemical Engineering 25 (2001) 571-576.

[8] N.M.S. Hasan, M.M.K. Khan, M.G. Rasul, A Study of Bubble Trajectory and Drag Co-efficient in Water and Non-Newtonian Fluids, WSEAS Transactions on Fluid Mechanics 3 (2008) 261-270.

[9] J. Magnaudet, M. Rivero, Accelerated flows past a rigid sphere or a spherical bubble. Part 1. Steady straining flow, Journal of Fluid Mechanics 284 (1995) 97-135.

[10] N. Hasan, Comparison of a computational model of single bubble collection efficiency in a hallimond tube, Seventh International Conference on CFD in the Minerals and Process Industries CSIRO, Melbourne, Australia (2009).